Enhanced flux pinning properties for GdBa$_2$Cu$_3$O$_{7-x}$ films with nanosized La$_{0.67}$Sr$_{0.33}$MnO$_3$ inclusions on SrTiO$_3$ substrate by RF magnetic sputtering method

Taobin Wang[1], Weilong Wang[1], and Ying Wang[1,2,*]

[1] *Department of Physics and Mathematics, Shanghai Key Laboratory of Materials Protection and Advanced Materials in Electric Power, Shanghai University of Electric Power, 1851# Hucheng Huan Road, Shanghai 201303, People's Republic of China*
[2] *Department of Materials Science, Fudan University, Shanghai 200433, People's Republic of China*

ABSTRACT

La$_{0.67}$Sr$_{0.33}$MnO$_3$ (LSMO) nanoparticles/SrTiO$_3$ (STO) structures were prepared as substrates using RF magnetron sputtering and GdBa$_2$Cu$_3$O$_{7-x}$ [(Gd)BCO] films were deposited on top. A significant improvement in superconductivity is observed under a magnetic field parallel to the GBCO H//c-axis. Due to the wider hysteresis loop, we observe that the Jc value of (Gd)BCO films on LSMO/STO remains at 1.0×10^5 A cm^{-2} at 77 K and 3 T magnetic field compared to 1.0×10^2 A cm^{-2} for (Gd)BCO films grown on bare STO. A significant enhancement of Fp and a shift of the [(Fp)max] magnetic field from 0.8 to 1.5 T. LSMO-induced defects and pinned Vortex properties in GdBa$_2$Cu$_3$O$_{7-x}$ matrix were investigated. We find that the formation of threading dislocation defects along the H//c-axis is the source of the improved induced properties in the GdBa$_2$Cu$_3$O$_{7-x}$ matrix.

1 Introduction

In the late 1980s, scientists have discovered copper oxide high-temperature superconductors(HTSs), which broke through the bottleneck of liquid nitrogen temperature [1–3]. Recently, a number of HTSs have been widely researched. As Tl-based HTS, (CuTl)$_{0.5}$Ba$_2$Ca$_2$Cu$_3$O$_{10-\delta}$\{(CuTl)-1223\} prepared from conventional solid-phase reactions suppressed the dielectric constant (ε_r', ε_r'') and loss tangent (tanδ)

and increased the AC conductivity (σ_{ac}) after the introduction of nanoparticles (NPs) such as Cr [4] and Cu [5]. As an iron-based superconductor (IBS) of high research value, the simplest member of the IBS family in terms of composition is FeSe ("11") [6, 7]. The FeSe compound is the simplest HTSs possible, and relatively cheap, not containing any rare-earth material [8]. In recent reports, Michael [9] et al. reported that the addition of Ag affects the superconductivity of the FeSe phase by improving

---

Taobin Wang and Weilong Wang were contributed equally to this manuscript.

Address correspondence to E-mail: 2006000081@shiep.edu.cn

Ⓐ Springer

connectivity and resistivity. $Bi_2Sr_2Ca_{n-1}Cu_{n+1}O_{2n+6}$ (BSCCO), which involves bismuth, strontium, calcium, and copper oxide, is an interesting class HTS of high-conductive systems [10]. For the first-generation superconducting tapes, BSCCO nanotapes have attracted great attention due to their easy fabrication process, and the numerous interconnects between the nanowires show a positive effect on the current flow and are essential for the superconducting performance. While the low irreversibility fields made them not suitable for applications in the strong magnetic field [11]. Then $(Re)Ba_2Cu_3O_7$ [(Re)BCO] tapes are considered to be the most promising candidate in power or AC application fields at 77 K, whereas the critical current density (Jc) for (Re)BCO films will decrease dramatically applied in a high magnetic field [12].

Vortex motion is the main mechanism for limiting the critical current density Jc in the mixed state. In previous reports, the only way to avoid vortex motion was to pin the vortex within the Abrikosov lattice. At the same time, the pinning problem is particularly important for HTS, where depinning occurs at temperatures close to Tc by a thermally activated process that grows exponentially with temperature. Among the previously effective approaches to enhance pinning in low- and high-temperature superconductors is the introduction of defects with nanoscale dimensions into the material. Due to the temperature dependence of the London penetration length (λ_L), condensation energy pinning or core pinning is dominant at low temperatures [13]. Furthermore, in the case of high-temperature superconductivity, condensation energy pinning is not high enough to avoid depinning due to thermal fluctuations due to the small size of the vortex core and the layered nature of HTS [14]. The decoration of non-magnetic NPs on the substrate surface and process enhancement are ways to improve the superconductivity of HTS. These non-magnetic materials include $CoFe_2O_4$, $BaZrO_3$, $BaSnO_3$, carbon nanotubes (CNTs), TiO_2, WO_3, SiO_2, and $YBaNbO_6$ [15–22], and so on. Recently, ball-milling techniques have been one of the most effective methods for preparing and improving the properties of various superconducting materials. Similar to the introduction of NPs to decorate HTS-induced structural defects, Hamrita [23] et al used ball-milling to cause fine particles with a particle size of approximately 15 nm to aggregate into coral-like agglomerates and embed themselves in

$YBa_2Cu_3O_{7-d}$. This modification of the fine structure helps to enhance the inter- and intra-crystalline critical current density Jc of the material under the influence of an applied magnetic field as well as enhancing the vortex flux pinning force Fp in the sample. Similarly, Slimani [24] found that the fine grain organisation of the $Y_3Ba_5Cu_8O_y$ bodies during high-energy ball-milling (HEBM) facilitated the enhancement of the critical current density and improved flux pinning ability. Various effective nanoscale magnetic inclusions have also been reported and showed improved in-field current-carrying ability owing to the magnetic character of the nanoinclusions [25–30]. Very recently, T. Petrisor [13] has observed enhanced pinning properties of $YBa_2Cu_3O_7$ (YBCO) films fabricated on $La_{1-x}Sr_xMnO_3$ (LSMO) film on a terraced (001) $SrTiO_3$ (STO) substrate. They believed that the normal core pinning mechanism together with a magnetic interaction pinning mechanism has contributed to the improvement.

$La_{0.67}Sr_{0.33}MnO_3$ NPs with ferromagnetic properties have been of great research value in previous applications [31, 32]. These LSMO nanoparticles themselves can act as magnetic pinning centres, allowing the decorated HTS to exhibit higher critical current density and flux pinning properties, hence our choice of LSMO ferromagnetic NPs as decorative materials. In this present investigation, we investigate the pinning characteristics of an $(Gd)Ba_2Cu_3O_7$ (Gd)BCO film deposited on LSMO nanosized particles-decorated STO substrate. Compared with YBCO, (Gd)BCO has a higher Jc and irreversibility field (Hirr) [33]. Therefore, we chose (Gd) BCO for the studied superconductor films. Two kinds of (Gd)BCO films were deposited: one is (Gd)BCO on LSMO-decorated STO and the other is (Gd)BCO on STO. For (Gd)BCO on LSMO-decorated STO, the enhanced flux pinning properties are observed up to a magnetic field of 3 T.

2 Experimental details

Using the JGP-560BD vacuum coating system with RF600C sputtering power supply, the $GdBa_2Cu_3O_{7-x}$[(Gd)BCO] films were grown on $La_{0.67}Sr_{0.33}MnO_3$ **(LSMO)** nanoparticles-decorated and bare (001) $SrTiO_3$ (STO) monocrystalline substrates. For the deposition of the LSMO on STO substrates, the

LSMO target(ϕ60mm $\times$ 4 mm) which was manufactured by Hefei Kejing Materials Technology Co. was sputtered with a total O_2(Purity 99.999%)/Ar(Purity 99.999%) mixed gas pressure of 25 Pa and the sputtering power was 80 W. The ratio of O_2/Ar and the substrate temperature were 1:1 and 780 °C, respectively. A sputtering time for 10 s was used. The growth parameters were identical for the growth of (Gd)BCO films on LSMO-decorated and bare (001) STO monocrystalline substrates. The deposited and the post-annealing procedures of (Gd)BCO films have been reported in our previous work [34]. The (Gd) BCO films were kept as 500 nm under the deposition time of 30 min. X-ray diffractometer (XRD) and atomic force microscopy (AFM) were employed to study the structural and the surface morphology of the LSMO NPs and (Gd) BCO films. The surface profilometer was used to measure film thickness, which is controlled by deposition time. The magnetotransport for (Gd) BCO films was obtained by a system of Quantum Design PPMS-9 T. At the same time, a four-probe technique with 1 µV/cm criterion was adopted to evaluate the Jc Values for (Gd) BCO films.

3 Results and discussion

In order to investigate the two- or three-dimensional surface morphologies of the LSMO-decorated STO substrates, the AFM analysis for the LSMO-decorated STO substrates has been done, and the results are shown in Fig. 1a–d. By varying the target–substrate distance from 30 to 50 mm, LSMO surface morphologies changed from LSMO NPs to LSMO nanowires together with nanoparticles. In Fig. 1a and b, the LSMO nanoparticles distribute randomly, with the diameter varying between 10 and 20 nm, when the target–substrate is 30 mm. Nevertheless, LSMO nanowires appear except for nanoparticles, with the target–substrate changed to 50 mm. The average length for LSMO nanowires is 210 nm. Because of a higher density and a smaller size of LSMO particles with a target–substrate of 50 mm, we intend to decorate STO with LSMO NPs and deposit (Gd)BCO films at this distance to investigate the effect of LSMO particles on the flux pinning properties on (Gd)BCO films.

For evaluating the phase composition and growth orientation of (Gd)BCO films grown on LSMO-decorated or bare STO, We performed XRD tests on samples in the 5°–60° range, with a step size of 0.02° and a wavelength range of 0.05–0.25 nm. XRD measurements were performed. Figure 1a and b presents the XRD θ–2θ scan patterns of the samples. Figure 1c shows the lattice structures of (Gd)BCO. (Gd)BCO has the layered perovskite structure, and its lattices parameters of a, b and c are 3.820 Å, 3.886 Å and 11.696 Å, respectively. It can be obviously seen from Fig. 1a and b that the two samples exhibit good (00l) preferential orientation. It indicates that there is hardly negative impact from the LSMO nanoparticles on STO for the (Gd)BCO films upon them. The small peaks at 29.2° and 33.3° are the (102) and (103), respectively. Due to low volume fraction of LSMO in the decorated sample, no peak corresponding to LSMO is observed in the XRD pattern of (Gd)BCO thin film fabricated on LSMO-decorated STO substrate. Interestingly, we found a very distinct diffraction peak in the STO/LSMO/(Gd)BCO structure above the (103) crystal orientation accompanied by the disappearance of the (102) peak in STO / (Gd)BCO structure. This is most likely due to the defects caused by the LSMO NPs during the deposition of the (Gd)BCO film. Furthermore, the change in cell parameters [35] caused by the doped LSMO NPs is essentially responsible for the change in intensity of the XRD peaks (e.g. 001, 002) (See Fig. 2).

The critical temperature of the two samples was determined from the intersection of the zero field-cooled (ZFC) magnetization measurements. The Tc for (Gd)BCO thin film fabricated on bared STO substrate was found to be 90.5 K, while for (Gd)BCO thin film deposited on LSMO-decorated STO, it was of 90.3 K. The magnetization hysteresis loop measurement was performed at 77 K, which is shown in Fig. 3. The applied magnetic field oriented in a direction parallel to the c-axis of the samples. The as-obtained magnetisation strength—magnetic field strength(M–H) loops were used to determine the critical current densities with Bean's critical state model [36]. By comparing the M–H and Jc–H curves for the (Gd)BCO film deposited directly on the LSMO-decorated STO and those for bare STO, two features may mainly be noted. First, as shown in Fig. 3a and b, the M-H loops for (Gd)BCO on LSMO-decorated STO have a bigger area over the whole studied magnetic field range at 77 K, compared with (Gd)BCO on STO. The second feature is related to the magnetic field dependence of the critical currents.

Fig. 1 **a** and **c** are the 2D atomic force microscopic images of LSMO nanoparticles and LSMO nanowires together with nanoparticles; **b** and **d** are the corresponding images of 3D atomic force microscopic images
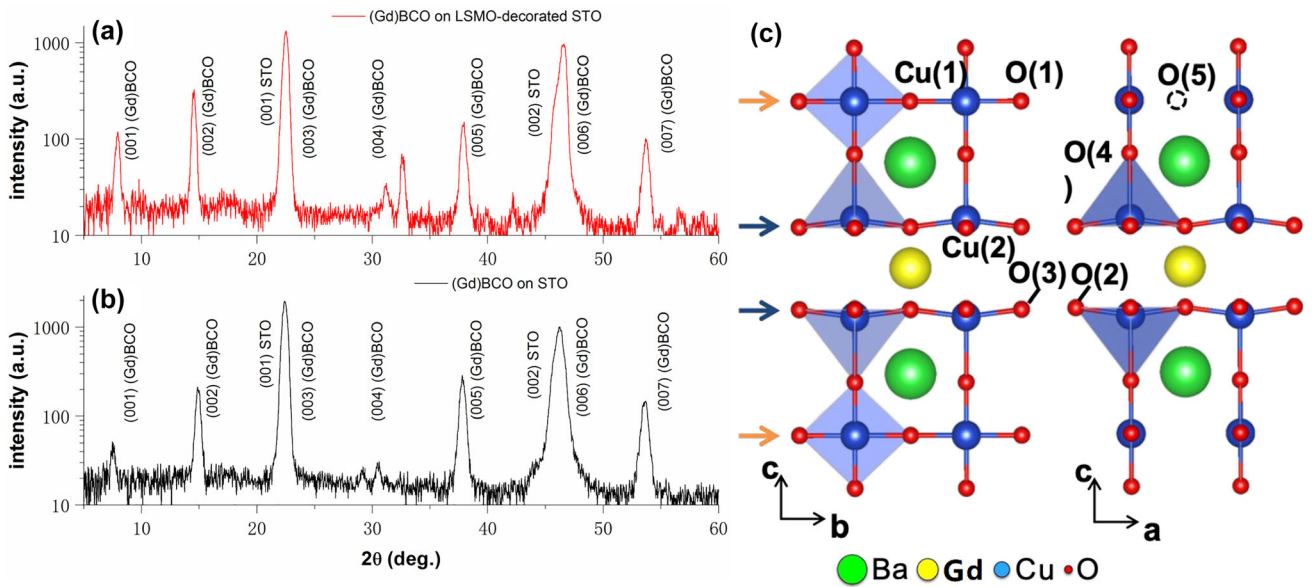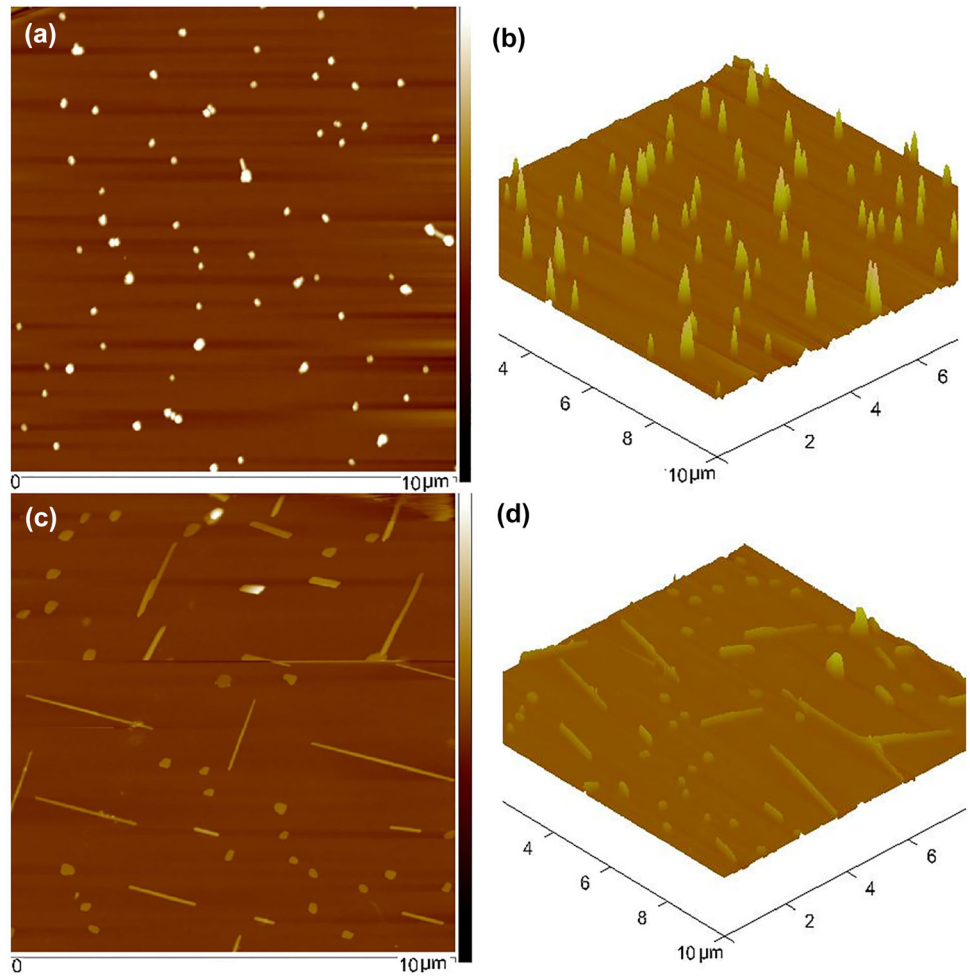
Fig. 2 XRD patterns of (Gd)BCO films on **a** LSMO-decorated STO **b** STO and **c** Lattice structure of (Gd)BCO crystal
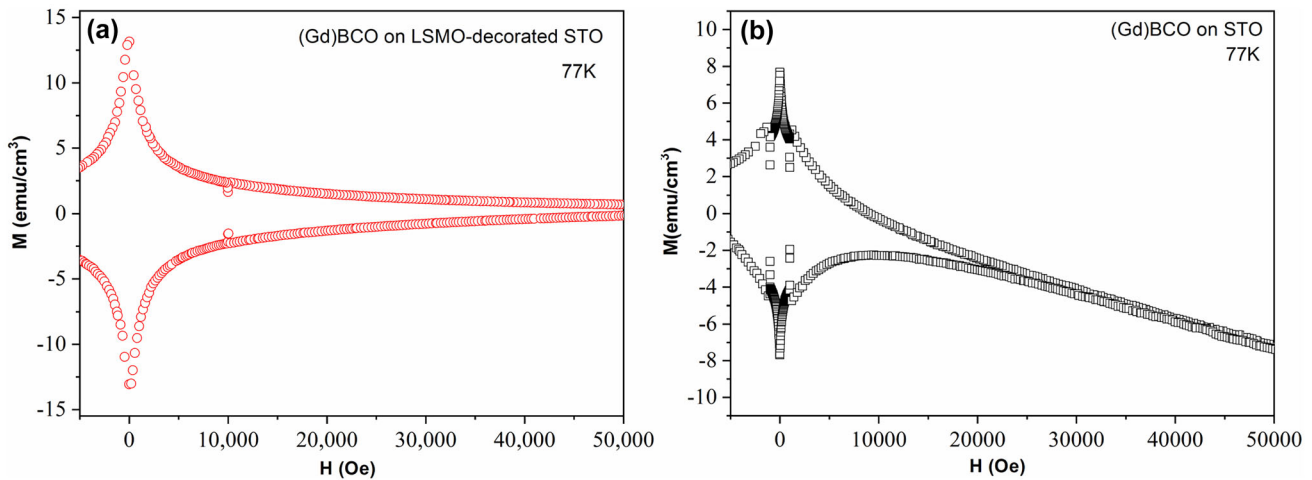
Fig. 3 M–H of (Gd)BCO films on **a** LSMO-decorated STO **b** STO

The critical current density (Jc) of the (Gd)BCO on LSMO-decorated STO and bare STO was evaluated by applying the modified Bean model[37] with the formula:

$$J_C = 2\Delta M \times [a(1 - a/3b)]^{-1}$$

where ΔM is the D-value between the upper and lower hysteresis loop at the same H, and a and b represent the dimensions of the prepared sample(the magnetic field is perpendicular to the sample plane, a ≤ b). Then the (Gd) BCO film grown on LSMO - decorated STO possess a larger Jc value over the whole studied region of magnetic field (77 K), which is shown in Fig. 4a.

It should be noted that improvements in Jc are usually manifested by correspondingly high quantitative values in high regions of the magnetic field [38] whereas, in our case, the Jc improvement also exists in the high region of magnetic field. At 77 K, the Jc value for (Gd)BCO on LSMO-decorated STO at an applied field of 1 T is 2.2×10^5 A cm^{-2}. But the Jc value for (Gd)BCO on STO is 1.0×10^5 A cm^{-2} for the same magnetic field of 1 T and the same temperature of 77 K. When the applied field increases to 3 T, the Jc value for (Gd)BCO on STO diminishes to 1.0×10^2 A cm^{-2}; meanwhile, the Jc value for (Gd)BCO on LSMO-decorated STO maintains at 1.0×10^5 A cm^{-2}.

The pinning force density (Fp) is another important parameter, which is used to evaluate the pinning potential strength, because stronger pinning potentials shift the corresponding magnetic field H [(Fp)-max] (maximum value of pinning force density) to

higher field. Figure 4b shows the variation of the pinning force density (Fp) as a function of the applied magnetic field for (Gd)BCO on LSMO-decorated STO and on bare STO. At 77 K, the [(Fp)max] value for (Gd)BCO on LSMO-decorated STO increased form 1.0 GN/m^2 to 3.0 GN/m^2, compared to (Gd)BCO on bare STO, a factor of 3 enhancement, which is an obvious evidence of the improved pinning properties for (Gd)BCO on LSMO-decorated STO. At the same time, the [(Fp)max] value shift from 0.8 T to more than 1.5 T for (Gd)BCO on LSMO-decorated STO and bare STO. It indicates the most effective flux pinning property move from low magnetic field region to high magnetic field region for (Gd)BCO on LSMO-decorated STO, relative to (Gd)BCO on bare STO.

We have also measured the Jc value of (Gd)BCO film on LSMO-decorated STO and bared STO at an applied magnetic field of 0.3 T and at 77 K. There are two magnetic field orientations for the measured Jc values : H//c-axis and H//a-b plane. For H//a-b plane, the Jc value for (Gd)BCO film on LSMO-decorated STO and bared STO was 4.5 MA/cm^2, and 4.0 MA/cm^2, respectively. For H//c-axis, the Jc value for (Gd)BCO film on LSMO-decorated STO and bared STO was 2.6 MA/cm^2, and 0.6 MA/cm^2, respectively. It should be noted that the maximum increase was observed for H//c-axis, compared with H//a-b plane. It implies that the pinning enhancement for LSMO nanoparticles is more effective along the c-axis.

The improvement in the flux pinning properties of (Gd)BCO thin films grown on non-magnetic nanoparticles-decorated substrates have been
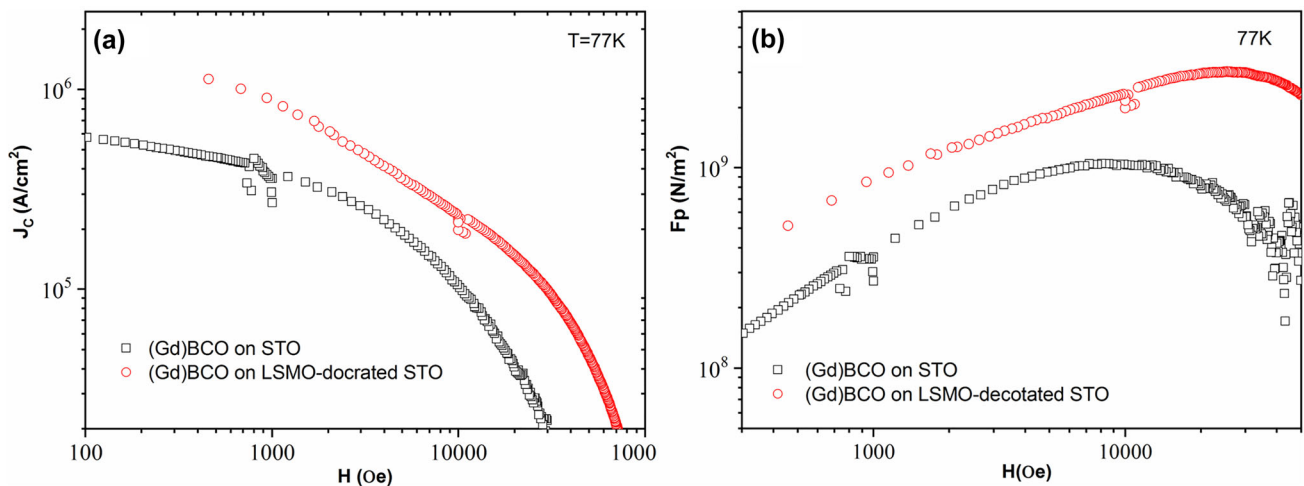
Fig. 4 **a** Jc–H of (Gd)BCO films on LSMO-decorated STO and STO **b** Fp–H of (Gd)BCO films on LSMO-decorated STO and STO

reported earlier. More than onefold enhancement in Jc value was achieved by growing YBCO film on Pd nanoparticles-decorated substrate [39]. Nie [40] has found that there is nearly 2-fold increment in Jc value at 2 T by CeO_2 nanoparticles decoration on substrate. As for (Gd)BCO films grown on LSMO-decorated STO, almost a four-fold increment in Jc value was observed at 6 T and 77 K, in our case. The previously reported enhancement of the self-field Jc in superconductors with ferromagnetic materials such as intercalated Fe_2O_3 [41], $YFeO_3$ [42], and so on might be explained by the Lorentz force affecting the pinning mechanism, where the forces generated by the transport currents that normally act only on (strong pinning) vortices are now separated between the vortices and the magnetic pinning sites themselves, thus allowing a greater current density to be built up before the vortices are dislodged [43].

It is well known that the (Fp) maxima are usually the same for non-magnetic nanoparticle-modified and controlled YBCO films. However, in our study, the (Fp) maxima changed from 0.8 to 1.5 T for (Gd)BCO on LSMO-decorated STO compared to (Gd)BCO on bare STO. This apparently different observation suggests a different pinning mechanism for (Gd)BCO films on LSMO-decorated STO compared to (Gd)BCO films on other non-magnetic nanoparticle-decorated substrates. The presence of non-magnetic NPs on the substrate is reported to introduce structural defects in the (Gd)BCO film resulting in enhanced flux pinning properties. A schematic representation of the structural defects along the c-axis in the (Gd)BCO film deposited on

LSMO-decorated STO is shown in Fig. 5. For LSMO-decorated (Gd)BCO films on STO, LSMO NPs can not only introduce structural defects in the form of nanoparticles, but can also lead to magnetic inhomogeneities. Magnetic inhomogeneity can also enhance the flux pinning properties of LSMO-modified (Gd)BCO films on STO. The self-built field at the centre of the driven flux pinning induced by LSMO makes the vortex motion more difficult through the Lorentz force, which leads to an enhancement of the critical current density Jc in the LSMO-decorated (Gd)BCO film. The presence of magnetic nanoparticles dictates that the flux quantum can be fixed around each magnetic nanoparticle. Therefore, for (Gd)BCO films deposited on LSMO NPs/STO substrates, there will be a large number of ferromagnetic/superconducting interfaces[32], which may
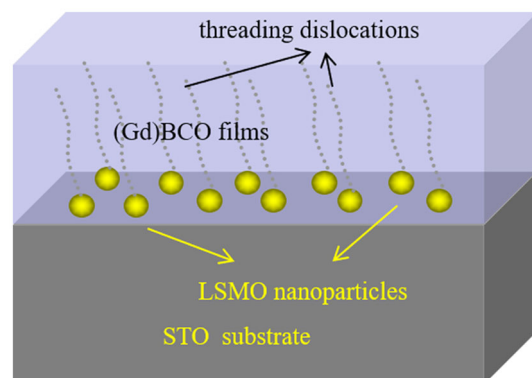
Fig. 5 Schematic diagram of structural defects generated along the c-axis in the (Gd)BCO film deposited on LSMO-decorated STO

result in samples with higher external magnetic field resistance strengths and hence the shift of (Fp)max towards higher magnetic fields that we observed in our tests.

4 Conclusions

In summary, we investigated the flux pinning properties of (Gd)BCO thin films deposited on LSMO nanoparticles/STO substrates. The introduction of LSMO nanoparticles at the (Gd)BCO/STO interface did not significantly change the transition temperature of the G(d)BCO films (only a 0.2 K drop). The LSMO nanoparticles acted as flux pinning centres and the resulting Lorentz force made it more difficult for vortices to operate, thus increasing the critical current density Jc of the (Gd)BCO films deposited on LSMO-decorated substrates. Applied magnetic field (3 T) was also observed for significantly higher film Jc (1.0×10^5 A cm^{-2}). It appears that the structural defects introduced by the ferromagnetic LSMO nanoparticles enhance the relevant pinning force properties on the H//c-axis, obtaining a shift in Fp (maximum) from 0.8 to 1.5 T.

Author contributions

All authors contributed to the study conception and design. Material preparation, data collection and analysis were performed by TW, WW and YW. The first draft of the manuscript was written by TW and WW and all authors commented on previous versions of the manuscript. All authors read and approved the final manuscript.

Funding

Data availability

Data sharing is not applicable to this article as no datasets were generated or analysed during the current study.

Declarations

Conflict of interest The authors have no relevant financial or non-financial interests to disclose.

References

1. M. Guidry, Y. Sun, Cl. Wu, Front. Phys. China **5**, 171–175 (2010)

2. K.A. Müller, A. Shengelaya, Dielectricly. J. Supercond. Nov. Magn. **26**, 491–493 (2013)

3. U. Chatterjee, D. Ai, J. Zhao et al., PNAS **23**, 9346–9349 (2011)

4. M. Mumtaza, L. Ali, Mubasher et al., Cryogenics **105**, 103021 (2020)

5. A. Abrar, M. Khan, J. Low. Temp. Phys. **199**, 1268–1298 (2020)

6. F.-C. Hsu, J.-Y. Luo, K.-W. Yeh et al., Proc. Natl. Acad. Sci. **105**, 14262 (2008)

7. Y. Mizoguchi, Y. Takano, J. Phys. Soc. Jpn. **79**, 102001 (2010)

8. Q. Nouailhetas, A. Koblischka-Veneva, M.R. Koblischka et al., AIP Adv. **11**, 015230 (2021)

9. M.R. Koblischka, Y. Slimani, A. Koblischka-Veneva et al., Materials **13**, 5018 (2020)

10. E. Hannachi, K.A. Mahmoud et al., Materials **3**, 1034 (2022)

11. M.R. Koblischka, A. Koblischka-V eneva, XianLin Zeng et al., Crystals **10**, 986 (2020)

12. G. Blatter, M.V. Feigelman, V.B. Geshkenbein et al., Rev. Mod. Phys. **66**(4), 1125–1388 (1994)

13. T. Petrisor Jr., M.S. Gabor, C. Tiusan et al., J. Appl. Phys. **112**, 5 (2012)

14. S.R. Foltyn, L. Civale, J.L. MacManus-Driscoll et al., Nature Mater. **6**, 631–642 (2007)

15. Y. Slimani, E. Hannachi, M.K. Ben Salem et al., J. Supercond. Nov. Magn. **28**, 3001–3010 (2015)

16. B. Maiorov, S.A. Baily, H. Zhou et al., Nat. Mater. **8**, 398–404 (2009)

17. E. Hannachi, M.A. Almessiere, Y. Slimani et al., J. Alloys Compd. **812**, 152150 (2020)

18. Y. Slimani, E. Hannachi, A. Ekicibil et al., J. Alloys Compd. **781**, 664–673 (2019)

19. Y. Slimania, M.A. Almessiere, E. Hannachi et al., Ceram. Int. **45**, 6828–7683 (2019)

20. M.K. Ben Salem, E. Hannachi, Y. Slimani et al., Ceram. Int. **40**, 4953–4962 (2014)

21. P. Mele, K. Matsumoto, T. Horide et al., Supercond. Sci. Tech. (2008). https://doi.org/10.1088/0953-2048/21/3/032002

22. D.M. Feldmann, T.G. Holesinger, B. Maiorov et al., Supercond. Sci. Tech. **23**, 115016 (2010)

23. A. Hamrita, Y. Slimani, M.K. Ben Salem et al., Ceram. Int. **40**, 1461–1470 (2014)

24. Y. Slimania, E. Hannachi, F. Ben Azzouz et al., Cryogenics **92**, 5–12 (2018)

25. J.H. Wimbush, R.B. Durrell et al., IEEE T Appl. Supercon. **3**, 3148–3151 (2009)

26. S.C. Wimbush, J.H. Durrell, C.F. Tsai et al., Sci. Technol. **23**, 045019 (2010)

27. A.V. Ushakov, I.V. Karpov, V.G. Demin et al., J. Mater. Sci: Mater. Electron. **30**, 15592–15598 (2019)

28. Xu. Kun, D. Zhou, B. Li et al., PHYSICA C **510**, 54–56 (2015)

29. M. Rekaby, Appl. Phys. A **126**, 664 (2020)

30. A.K. Jha, K. Matsumoto, T. Horide et al., J. Appl. Phys. **122**, 093905 (2017)

31. J. Gutierrez, T. Puig, M. Gibert, C. Moreno et al., Appl. Phys. Lett. **94**, 172513 (2009)

32. A.K. Jha, N. Khare, R. Pinto, J. Appl. Phys. **110**, 113920 (2011)

33. D.H. Tran, W.B.K. Putri, C.H. Wie et al., Thin Solid Films **526**, 241–245 (2012)

34. Z. Xie, Z. Li, H. Lu, Y. Wang et al., J. Mater. Sci: Mater. Electron. **31**, 19056–19063 (2020)

35. F. Touri, A. Sahari, A. Zouaoui et al., Surf. Rev. Lett. **27**, 1950114 (2020)

36. R. Bean, Mod. Phys. **1**, 31–39 (1964)

37. E.M. Gyorgy, R.B. van Dover, K.A. Jackson et al., Appl. Phys. Lett. **55**, 283 (1989)

38. M. Tange, R. Yoshizaki, J. Phys. Soc. Jpn. **78**, 024703 (2009)

39. J.H. Kwon, Y.F. Meng, L.J. Wu et al., Supercond. Sci. Technol. **31**, 105006 (2018)

40. J.C. Nie, Z.Y. Hua, Q.Y. Tu et al., PHYSICA C **460**, 1353–1354 (2007)

41. J. Wang, C.-F. Tsai, Z. Bi et al., IEEE T Appl. Supercon. **3**, 3503–3506 (2009)

42. S.C. Wimbush, J.H. Durrell, C.F. Tsai et al., Supercond. Sci. Technol. **23**, 045019 (2010)

43. M.G. Blamire, R.B. Dinner, S.C. Wimbush et al., Supercond. Sci. Technol. **22**, 025017 (2009)